SUPPORTING INFORMATION

Geometry as a Catalyst: How Vapor Cavities Nucleate from Defects

Alberto Giacomello,[†] Mauro Chinappi,[‡] Simone Meloni,[¶,§] and Carlo Massimo Casciola[*,†]

Dipartimento di Ingegneria Meccanica e Aerospaziale, Sapienza Università di Roma, Rome, Italy, Center for Life Nano Science@Sapienza, Istituto Italiano di Tecnologia, Rome, Italy, and CINECA Consortium, Rome, Italy

E-mail: carlomassimo.casciola@uniroma1.it

Phone: +39 0644585201. Fax: +39 06484854

The present Supporting Information is divided into three sections. The first one deals with the computational methods and setup parameters of the molecular dynamics (MD) simulations. In particular the restrained molecular dynamics method and the simulations protocols for the determination of surface tension, contact angle, and depletion layer are described. The second section is dedicated to cavitation on hydrophilic surfaces. Technical details on the master equations for the determination of the nucleation rate are reported in the last section.

[*]To whom correspondence should be addressed

[†]Dipartimento di Ingegneria Meccanica e Aerospaziale, Sapienza Università di Roma, Rome, Italy

[‡]Center for Life Nano Science@Sapienza, Istituto Italiano di Tecnologia, Rome, Italy

[¶]CINECA Consortium, Rome, Italy

[§]Laboratory of Computational Chemistry and Biochemistry, Institute of Chemical Science and Engineering, École Polytechnique Fédérale de Lausanne, Lausanne, Switzerland

1 Molecular dynamics simulation

1.1 Restrained Molecular Dynamics (RMD) for estimating free energy

In this section we quickly summarize the system set-up and method we used to compute the free energy profile from atomistic simulations, for further details on the subject refer to.[1]

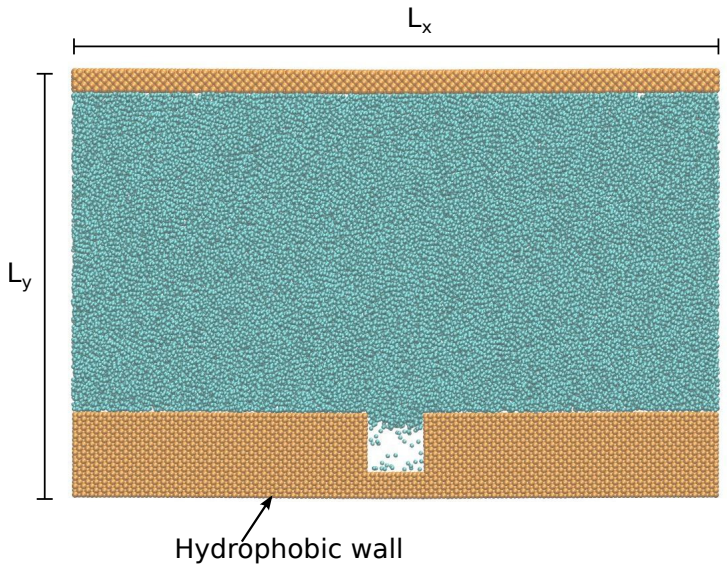

Figure S1: Snapshot from a RMD simulation. The wall atoms are represented as orange spheres while the liquid is reported in cyan.

System set-up. In the main text we compare MD and CREaM results. This comparison is performed considering the case of a Lennard-Jones liquid (LJ) confined between two hydrophobic planar walls with a nanoscale rectangular groove on one of them, see Fig. S1. The solid walls are formed by LJ atoms in FCC configuration, interacting with the liquid via the modified LJ potential $v(r) = 4\epsilon[(\sigma/r)^{12} - c(\sigma/r)^6]$, where ϵ defines the energy scale, σ the length scale, r is the interatomic distance and the parameter c is used to tune the hydrophobicity of the walls. Along with the mass of the atoms, σ and ϵ completely specify all the fundamental quantities (density, pressure, time...) in the simulation. As usually done for LJ systems, in our simulations these three parameters are set to unity and "dimensionless"

quantities are always referred to. We set $c = 0.6$, corresponding to a Young contact angle $\theta_{\rm Y} \simeq 112^\circ$ (see following section). The simulation box is a parallelepiped of average size $118 \times 72 \times 11$; the average distance between the two confining walls is 53. The groove where nucleation is simulated is around $11 \times 11 \times 11$, i.e., about 10 times the LJ atoms size.

RMD. Let us consider a microscopic observable $\theta(\mathbf{r})$, where $\mathbf{r}$ denotes an atomistic configuration. The probability density to find the system in a configuration in which $\theta(\mathbf{r}) = z$ is $P_\theta(z) = \int dV \int d\mathbf{r}\ \mu(\mathbf{r}, V)\delta(\theta(\mathbf{r}) - z)$, where $\mu(\mathbf{r}, V)$ is the equilibrium distribution of the system, that here we assume to be the one corresponding to the ensemble at constant number of particles, temperature, and pressure (NPT). The (Landau) free energy is defined as $G_\theta(z) = -\beta^{-1} \log P_\theta(z)$, with $\beta = 1/(k_{\rm B}T)$. A naive approach for computing the free energy consists in running a long MD simulation, building the histogram of $\theta(\mathbf{r})$ along it, which is an estimate of $P_\theta(z)$, and from this evaluate $G_\theta(z)$. However, in case of rare events this approach is unsuitable because the regions having low probability, around the transition state, are visited too infrequently (in many cases never over the typical timescale of atomistic simulations). Techniques for dealing with this problem consist in forcing the system to visit the low probability regions. Here we use an approach derived from the Temperature Accelerated MD method.[2] In short, we replace $\delta(\theta(\mathbf{r}) - z)$ in the definition of $P_\theta(z)$ with the Gaussian $\sqrt{\beta k/2\pi} \exp[-(\theta(\mathbf{r}) - z)^2 \beta k/2]$, which converges to the Dirac delta, δ, in the limit $\beta k \to \infty$. Thus, the derivative of the free energy can be approximated by

$$\frac{dG_\theta(z)}{dz} \simeq -\frac{\int dV \int d\mathbf{r}\ k(\theta(\mathbf{r}) - z)\mu(\mathbf{r}, V) \exp[-\frac{\beta k}{2}(\theta(\mathbf{r}) - z)^2]}{\int dV \int d\mathbf{r}\ \mu(\mathbf{r}, V) \exp[-\frac{\beta k}{2}(\theta(\mathbf{r}) - z)^2]}\,. \tag{1}$$

This approximate formula can be recast into the ensemble average of the observable $-k(\theta(\mathbf{r}) - z)$ over the biased distribution $\mu'(\mathbf{r}, V) = \exp[-\beta(U(\mathbf{r}) + k/2(\theta(\mathbf{r}) - z)^2 + PV)]/\mathcal{Q}(z)$, where $U(\mathbf{r})$ is the physical potential and $\mathcal{Q}(z)$ is the normalization factor. The above ensemble average can be estimated *via* NPT MD simulations[3] driven by the biased potential $U(\mathbf{r}) +$

$k/2(\theta(\mathbf{r})-z)^2$. Finally, the free energy profile $G_\theta(z)$ can be obtained numerically integrating $dG_\theta(z)/dz$.

The collective variable $\theta(\mathbf{r})$ used in the present work counts the number of particles m in a box around the groove. This can be expressed using the characteristic function $\chi(\mathbf{r})$, which is equal to 1 if $\mathbf{r}$ is in the box and 0 otherwise: $\theta(\mathbf{r}) = \sum_{\mathrm{i}=1}^{N} \chi(\mathbf{r}_\mathrm{i})$, where $\mathbf{r}_\mathrm{i}$ is the position of the i-th particle and N is the number of liquid particles in the sample. In turn, the characteristic function can be expressed as the product of Heaviside step functions: $\chi(\mathbf{r}) = H(x^u - x)H(x - x^l)H(y^u - y)H(y - y^l)$, where x^u and x^l, and y^u and y^l are the upper and lower bounds of the box in the x and y direction, respectively. This form of the collective variable is unsuitable for our purposes as it produces impulsive forces on the particles as they cross the boundaries of the box (the force associated to the biasing potential depends on $\nabla\theta(\mathbf{r})$). This problem is solved by replacing the Heaviside step function with a smooth approximation. In particular, we use an approximation based on the Fermi function $f(s) = 1 - 1/(\exp(cs) + 1)$, where c is a parameter controlling the steepness of $f(s)$ ($c = 3$ in our simulations).

Free energy profiles as a function of m obtained from MD simulation cannot be directly compared with free energy profiles as a function of V_v obtained from CREaM. The relation between m and V_v is $V_\mathrm{v} = (N_\mathrm{box} - m)/\rho_\mathrm{l}$, where N_box is the number of particle in the box around the groove when the system is in the fully wet Wenzel state, and ρ_l is the bulk density of the liquid. Another detail that must be addressed in comparing atomistic and CREaM results is the size of the system the free energy refers to. The free energy computed in the atomistic simulation is relative to a periodic slice of (average) thickness 11 (in the direction perpendicular to the page in Fig. S1). The CREaM grand potential reported in the main text is therefore referred to the same slice.

A further comment concerns the determination of ΔP in our atomistic simulations, to be used as input parameter in the CREaM calculations reported in Fig. 2 of the main text. This datum is not readily available in our simulation, in which we fix only the total pressure

of the system. We obtain ΔP by computing the average value of the pressure in two control-volumes in the vapor and liquid domains following an approach *à la* Irving and Kirkwood.[4] Obviously, this is possible only when the groove is not completely wet; in these cases, we observe that the value of ΔP is practically constant with respect to the box filling m.

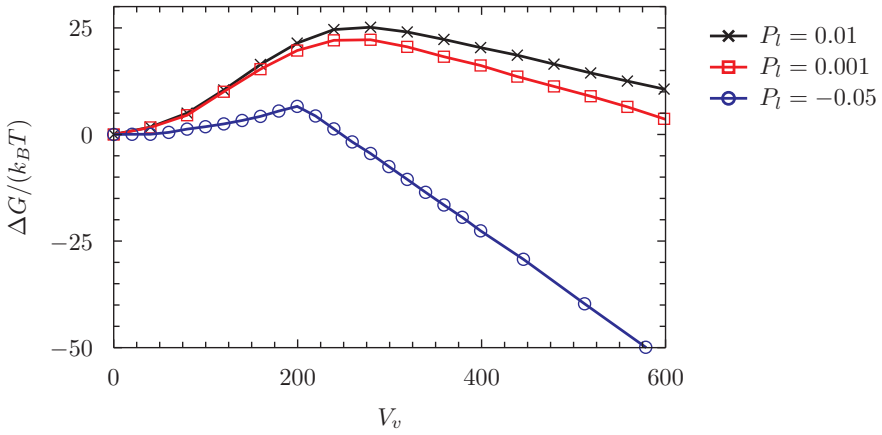

Figure S2: Free energy profiles from RMD simulations of the groove geometry in Fig. S1, the same used in the main text, for two different values of liquid pressure $P_\mathrm{l} = 0.001$ and $P_\mathrm{l} = 0.01$. A curvature change is apparent in the first branch of the curve at $V \simeq 100$. The maxima at $V \simeq 250$ correspond to the configuration change from asymmetric (bubble in the corner) to symmetric meniscus. The pressure $P_\mathrm{l} = -0.05$ is the same of Fig. 2 of the main text and is reported here for comparison.

As anticipated in the main text, in Fig. S2 we report free energy profiles obtained from atomistic simulations for the groove geometry at different values of the liquid pressure, namely $P_\mathrm{l} = 0.001$ and $P_\mathrm{l} = 0.01$. Differently from the case of Fig. 2 of the main text and reported in blue in Fig. S2, the free energy profiles at these pressures present a curvature change in the first branch ($V_\mathrm{v} < 250$). The small V_v range ($V_\mathrm{v} \leq 100$), where the free energy profile presents a positive curvature, is associated with a state in which the bubble in the corner is not yet formed. Rather, a liquid depletion is observed at the bottom wall of the groove (see upper right panel of Fig. 2 of the main text). In the second range ($100 < V_\mathrm{v} < 250$), where the $\Delta\Omega$ presents a negative curvature as predicted by CREaM, the bubble in the corner is, indeed, formed.

1.2 Liquid-vapor surface tension

The liquid-vapor surface tension γ_{lv} (used in CREaM for the comparison with restrained MD results) is computed using the Kirkwood *et al.* approach.[5] A two phase LJ liquid-vapor system is simulated in a triperiodic box, the interface being parallel to the Oxz plane. In this MD set-up the surface tension γ_{lv} reads:[6]

$$\gamma_{\mathrm{lv}} = \frac{L_{\mathrm{y}}}{2}\left(P_{\mathrm{N}} - P_{\mathrm{T}}\right) \tag{2}$$

where the factor 1/2 follows because of the presence of two interfaces and P_{N} and P_{T} are the normal and tangential components of the pressure tensor $P_{\alpha\beta}$:

$$P_{\mathrm{N}} = P_{\mathrm{yy}} = \frac{\rho_{\mathrm{l}}}{\beta} + \frac{1}{V}\left\langle \sum_{\mathrm{i,j>i}} y_{\mathrm{ij}} f_{\mathrm{ij}}^{y} \right\rangle \tag{3}$$

and

$$P_{\mathrm{T}} = \frac{P_{\mathrm{xx}} + P_{\mathrm{zz}}}{2} = \frac{\rho_{\mathrm{l}}}{\beta} + \frac{1}{2V}\left\langle \sum_{\mathrm{i,j>i}} x_{\mathrm{ij}} f_{\mathrm{ij}}^{x} + z_{\mathrm{ij}} f_{\mathrm{ij}}^{z} \right\rangle \tag{4}$$

where f_{ij}^{x}, f_{ij}^{y}, and f_{ij}^{z} are the pair force components between atoms i and j in the x, y, and z direction, respectively. x_{ij}, y_{ij} and z_{ij} are the three components of the difference of the positions of the atoms i and j. The symbol $\langle\cdot\rangle$ denotes an ensemble average over the canonical ensemble, which we estimate *via* a Langevin MD simulation.

1.3 Contact angle

To compute the Young contact angle θ_{Y} we deposited a cylindrical drop of LJ liquid on a flat surface parallel to the Oxz plane. The characteristics of the surface and of the liquid-surface interaction are the same used throughout and described above. The cylindrical shape of the drop is obtained by using a thin simulation box. The advantage of this set-up compared with the sessile spherical drop (see e.g.[7,8]) is that the length of the triple line does not depend on the size of the drop and, consequently, the line-tension contribution to energy balance and

droplet radius does not enter in the θ_Y expression.[9]

Consider the normalized density field $\rho^*(x, y)$:

$$\rho^*(x, y) = \frac{\rho(x, y) - \rho_v^B}{\rho_l^B - \rho_v^B} \tag{5}$$

where $\rho(x, y)$ is the density at the point (x, y). ρ_v^B and ρ_l^B are the bulk densities of the vapor and the liquid phases, respectively. $\rho^*(x, y)$ goes from 1 in the bulk of the liquid to 0 in the bulk of the vapor. The droplet surface S is defined as $S = \{(x, y) : \rho^*(x, y) = 0.5\}$. S is fitted with a circumference and from the angle formed by its tangent at the triple line with the solid surface we obtain θ_Y, which in the present case is $\sim 112°$.

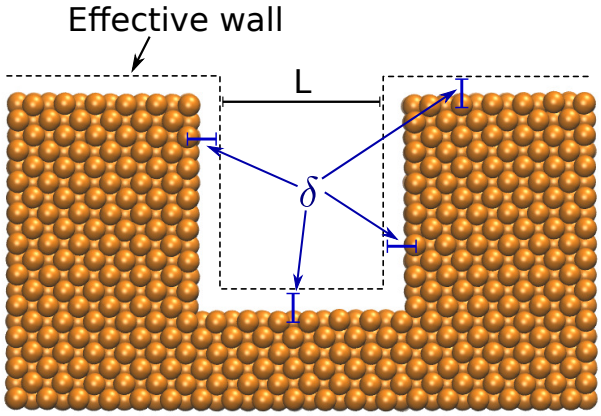

Figure S3: Depletion layer and effective wall position. The solid LJ atoms are represented as orange spheres. The effective wall is at a distance δ from the "surface" atoms of the solid.

1.4 Depletion layer

Another parameter used as an input to CREaM is the size of the surface corrugation, the width L of the cavity in the case of the groove. This quantity is not clearly defined in atomistic systems. A possibility is defining L as the distance between the "surface" atoms on the opposite walls of the groove. However, for hydrophobic surfaces, due to the low affinity between the solid and the liquid, a local depletion layer of length δ is observed, shifting the

solid-liquid interface towards the liquid. Thus, the effective wall position is that shown with a dashed line in Fig. S3, with the associated corrugation length L encompassing δ. Following Janecek and Netz,[10] δ is defined as:

$$\delta = \int_{-\infty}^{\infty} \left[1 - \frac{\rho_{\mathrm{l}}(y)}{\rho_{\mathrm{l}}^{B}} - \frac{\rho_{\mathrm{s}}(y)}{\rho_{\mathrm{s}}^{B}} \right] \mathrm{d}y \tag{6}$$

where l denotes the liquid phase, s the solid phase. To evaluate δ we perform a NVT simulation of a triperiodic system constituted by a solid and a liquid slab parallel to Oxz plane. Solid-liquid interactions are the same discussed in previous sections. From the NVT simulation we obtain the fields $\rho_{\mathrm{l}}(y)$ and $\rho_{\mathrm{s}}(y)$ that we plug into Eq. (6). The resulting depletion layer is $\delta = 0.52$.

2 Hydrophilic crevices

In some cases, discussed below, even hydrophilic surface defects can increase rates as compared to nucleation in the bulk and on a flat surface. By definition, hydrophilic surfaces have $\theta_{\mathrm{Y}} < \pi/2$. This means that the crevice angle β is always larger than $2\theta_{\mathrm{Y}} - \pi$, which implies that we always fall in the wide crevice case. For $\theta_{\mathrm{Y}} \geq \beta/2$ the curvature *vs* volume diagram is qualitatively similar to that shown in Fig. 1b of the main text, the major difference being that the minimum of $\tilde{j}(\tilde{v}_{\mathrm{v}})$ (at the pinned-outside regions boundary for the hydrophobic case) here moves inside the pinned region. For $\theta_{\mathrm{Y}} < \beta/2$, $\tilde{j}(\tilde{v}_{\mathrm{v}})$ changes shape, becoming monotonically growing. This implies that the system presents only two metastable states, Wenzel and vapor, and a single barrier regardless of the value of N_{nu}.

In Fig. S4, top panel, we report the free energy barriers relative to the bulk barrier, $\Delta\tilde{\tilde{\omega}}_{*}^{\dagger} \equiv \Delta\Omega_{*}^{\dagger}/\Delta\Omega_{\mathrm{b}}^{\dagger}$, against the nucleation number, N_{nu} for a case where $\theta_{\mathrm{Y}} > \beta/2$. For this value ($\theta_{\mathrm{Y}} = 0.4\,\pi$ and $\beta = 0.4\pi$), crevices have a catalytic effect for all N_{nu}. For $\theta_{\mathrm{Y}} = 0.15\,\pi$, at sufficiently large nucleation numbers, the free energy barrier on a single defect are lower than in the bulk or on a flat surface. For $\theta_{\mathrm{Y}} = 0.1\,\pi$, nucleation in the crevice is always

unfavorable as compared to nucleation on a flat surface having the same contact angle.

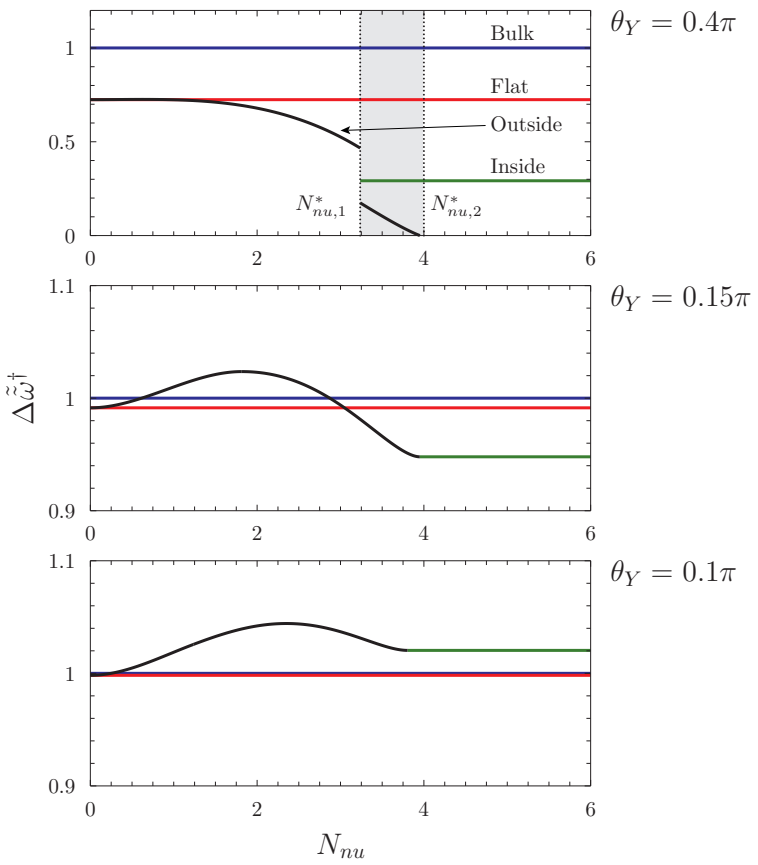

Figure S4: Forward free energy barriers (defined as in Fig. 3 of the main text) for hydrophilic conical crevices, as a function of the nucleation number $N_{\rm nu} \equiv -L\Delta P/\gamma_{\rm lv}$. The cone angle is taken to be $\beta = 0.4\pi$ for all panels. The shaded region in the top panel denotes the range where nucleation is a two-steps process (three metastable states).

3 Computation of the nucleation rate

In this section we discuss the calculation of the characteristic time, τ, of the cavitation process that we used in the main text to derive the catalytic effect of a surface textured with wide hydrophobic crevices, $\alpha = \tau_{\rm flat}/\tau_{\rm crev}$ ($\tau_{\rm flat}$ and $\tau_{\rm crev}$ denote the characteristic times of flat and textured surfaces, respectively).

Following the results presented in the main text, the most general set of master equations

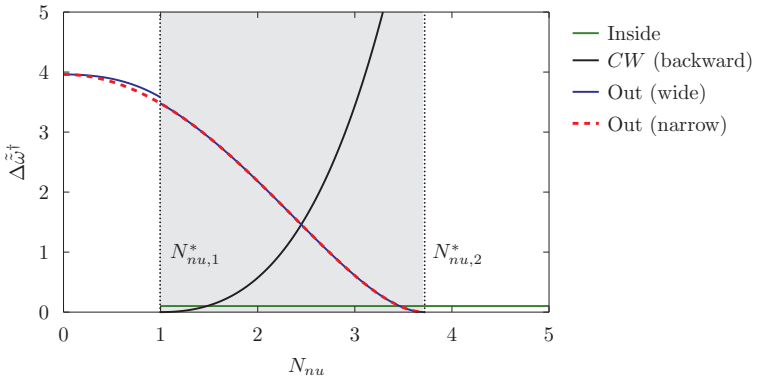

Figure S5: Nondimensional free energy barriers $\Delta\tilde{\omega}^{\dagger}$. Solid lines denote the wide crevice forward (green and blue) and backward (black) free energy barriers. The dashed line denotes the only barrier present in the narrow crevice case, occurring outside the crevice. The vertical dotted lines identify the range $N^*_{\mathrm{nu},1} < N_{\mathrm{nu}} < N^*_{\mathrm{nu},2}$ (shaded) where nucleation is a two-step process.

governing the time evolution of the system is:

$$\dot{p}_{\mathrm{W}}(t) = -k_{\mathrm{WC}}p_{\mathrm{W}} + k_{\mathrm{CW}}p_{\mathrm{C}} \ , \tag{7a}$$

$$\dot{p}_{\mathrm{C}}(t) = k_{\mathrm{WC}}p_{\mathrm{W}} - (k_{\mathrm{CW}} + k_{\mathrm{CV}})p_{\mathrm{C}} + k_{\mathrm{VC}}p_{\mathrm{V}} \ , \tag{7b}$$

$$\dot{p}_{\mathrm{V}}(t) = k_{\mathrm{CV}}p_{\mathrm{C}} - k_{\mathrm{VC}}p_{\mathrm{V}} \ , \tag{7c}$$

with p_{a} the probability to be in the state a, and k_{ab} the transition rate from a to b. $p_{\mathrm{a}} = \int_{\mathcal{V}_{\mathrm{a}}} dz\, P_{\theta}(z)$, i.e. is the integral of the probability density introduced above over the z-space volume identifying the state a, $\mathcal{V}_{\mathrm{a}}$. The indices W, C and V indicate the Wenzel, Cassie and Vapor phases, respectively. The sum of the probabilities to be in the Wenzel, Cassie and vapor states is almost equal to one, reflecting the fact that the system spends almost all the time in one of the metastable states. For the sake of simplicity, we assume that the above probabilities obey the relation $p_{\mathrm{W}}(t) + p_{\mathrm{C}}(t) + p_{\mathrm{V}}(t) = 1$. This implies that only two of the Eqs. (7) are independent.

When the system features only two metastable states, Wenzel and vapor, Eqs. (7) reduce

to the set:

$$\dot{p}_{\mathrm{W}}(t) = -k_{\mathrm{WV}} p_{\mathrm{W}} + k_{\mathrm{VW}} p_{\mathrm{V}} \ , \tag{8a}$$

$$\dot{p}_{\mathrm{V}}(t) = k_{\mathrm{WV}} p_{\mathrm{W}} - k_{\mathrm{VW}} p_{\mathrm{V}} \ . \tag{8b}$$

Consider a system with a wide crevice prepared in the Wenzel state, $p_{\mathrm{W}}(0) = 1$. For $N_{\mathrm{nu}} < N^*_{\mathrm{nu},1}$ the system presents only two metastable states, Wenzel and vapor, see the single associated barrier $\Delta\tilde{\bar{\omega}}^{\dagger}_{\mathrm{out}}$ in Fig. S5 (solid blue line). Given the initial conditions, $p_{\mathrm{W}}(t) = \exp[-t/\tau]$, where the characteristic time is $\tau = 1/(k_{\mathrm{WV}} + k_{\mathrm{VW}})$. However, since k_{VW} is negligible, $\tau = 1/(k_{\mathrm{WV}})$. k_{WV} corresponds to the barrier denoted as "outside" in Fig. 3 of the main text. Thus, for consistency of notation, we call $k_{\mathrm{WV}} = k_{\mathrm{out}}$ and $\tau = 1/(k_{\mathrm{out}})$.

When $N^*_{\mathrm{nu},1} < N_{\mathrm{nu}} < N^*_{\mathrm{nu},2}$ the system is characterized by three metastable states, and the kinetics of the systems is described by the master equations (7). Neglecting the vanishingly small term k_{VC}, the solution of this set of differential equations is

$$p_{\mathrm{v}}(t) = 1 + \frac{\lambda_2}{\sqrt{\Delta}} \mathrm{e}^{\lambda_1 t} - \frac{\lambda_1}{\sqrt{\Delta}} \mathrm{e}^{\lambda_2 t} \ , \tag{9}$$

where $\lambda_{1,2}$ are the eigenvalues of the reduced set of two differential equations obtained combining Eq. (7) with the conservation of the total probability and $\Delta = (k_{\mathrm{CW}} + k_{\mathrm{CV}} + k_{\mathrm{WC}})^2 - 4k_{\mathrm{WC}}k_{\mathrm{CV}}$. The eigenvalues (both negative) read:

$$\lambda_{1,2} = \frac{-(k_{\mathrm{CW}} + k_{\mathrm{CV}} + k_{\mathrm{WC}}) \pm \sqrt{\Delta}}{2} \ .$$

Equation (9) has a double exponential form, however, with the actual values calculated for the k_{WC}, k_{CV} and k_{CW} rates the prefactor of the $e^{\lambda_2 t}$ term results negligible. Moreover, since $|\lambda_1| \ll |\lambda_2|$, the $e^{\lambda_2 t}$ term quickly converges to zero and, hence, the governing timescale of the nucleation process is $\tau = 1/\lambda_1$.

Finally, for $N_{\mathrm{nu}} > N^*_{\mathrm{nu},2}$ the system is once again two-states, with a single barrier corresponding to a transition state in which the liquid-vapor interface is inside the crevice, $\Delta\tilde{\tilde{\omega}}^{\dagger}_{\mathrm{in}}$ (see green lines in Fig. 4a in the main text and Fig. S5). Here, like in the first region, the backward rate is negligible as compared to the forward one and, using the notation adopted in the main text, the characteristic time is $\tau = 1/k_{\mathrm{in}}$.

For the case of smooth surfaces we have only a one-step process (two metastable states), and the characteristic time is $\tau = 1/(k_{\mathrm{WV}} + k_{\mathrm{VW}})$, where here W stands for *wet*. Like in the case of textured surfaces, k_{VW} is negligible and $\tau = 1/k_{\mathrm{WV}}$.

References

(1) Tuckerman, M. *Statistical Mechanics and Molecular Simulations*; Oxford University Press, 2008.

(2) Maragliano, L.; Vanden-Eijnden, E. A temperature accelerated method for sampling free energy and determining reaction pathways in rare events simulations. *Chemical Physics Letters* **2006**, *426*, 168–175.

(3) Martyna, G. J.; Tobias, D. J.; Klein, M. L. Constant pressure molecular dynamics algorithms. *The Journal of Chemical Physics* **1994**, *101*, 4177.

(4) Irving, J. H.; Kirkwood, J. G. The statistical mechanical theory of transport processes. IV. The equations of hydrodynamics. *The Journal of Chemical Physics* **1950**, *18*, 817.

(5) Kirkwood, J. G.; Buff, F. P.; Green, M. S. The statistical mechanical theory of transport processes. III. The coefficients of shear and bulk viscosity of liquids. *The Journal of Chemical Physics* **1949**, *17*, 988.

(6) Gloor, G. J.; Jackson, G.; Blas, F. J.; de Miguel, E. Test-area simulation method for the direct determination of the interfacial tension of systems with continuous or discontinuous potentials. *The Journal of chemical physics* **2005**, *123*, 134703–134703.

(7) Giacomello, A.; Meloni, S.; Chinappi, M.; Casciola, C. Cassie-Baxter and Wenzel States on a Nanostructured Surface: Phase Diagram, Metastabilities, and Transition Mechanism by Atomistic Free Energy Calculations. *Langmuir* **2012**, *28*, 10764–10772.

(8) Chinappi, M.; Casciola, C. Intrinsic slip on hydrophobic self-assembled monolayer coatings. *Physics of Fluids* **2010**, *22*, 042003.

(9) Weijs, J. H.; Marchand, A.; Andreotti, B.; Lohse, D.; Snoeijer, J. H. Origin of line tension for a Lennard-Jones nanodroplet. *Physics of Fluids* **2011**, *23*, 022001–022001.

(10) Janecek, J.; Netz, R. R. Interfacial water at hydrophobic and hydrophilic surfaces: Depletion versus adsorption. *Langmuir* **2007**, *23*, 8417–8429.